Atmos. Meas. Tech. Discuss., 8, 3967–4009, 2015
www.atmos-meas-tech-discuss.net/8/3967/2015/
doi:10.5194/amtd-8-3967-2015
© Author(s) 2015. CC Attribution 3.0 License.

Atmospheric Measurement Techniques Discussions
Open Access

This discussion paper is/has been under review for the journal Atmospheric Measurement Techniques (AMT). Please refer to the corresponding final paper in AMT if available.

Spatial mapping of ground-based observations of total ozone

K.-L. Chang[1], **S. Guillas**[1], **and V. E. Fioletov**[2]

[1]Department of Statistical Science, University College London, London, UK
[2]Environment Canada, Toronto, Ontario, Canada

Received: 26 January 2015 – Accepted: 20 March 2015 – Published: 22 April 2015

Correspondence to: K.-L. Chang (ucakkac@ucl.ac.uk)

Published by Copernicus Publications on behalf of the European Geosciences Union.

Abstract

Total column ozone variations estimated using ground-based stations provide important independent source of information in addition to satellite-based estimates. This estimation has been vigorously challenged by data inhomogeneity in time and by the irregularity of the spatial distribution of stations, as well as by interruptions in observation records. Furthermore, some stations have calibration issues and thus observations may drift. In this paper we compare the spatial interpolation of ozone levels using the novel stochastic partial differential equation (SPDE) approach with kriging. We show how these new spatial predictions are more accurate, less uncertain and more robust. We construct long-term zonal means to investigate the robustness against the absence of measurements at some stations as well as instruments drifts. We conclude that time series analyzes can benefit from the SPDE approach compared to kriging when stations are missing, but the positive impact of the technique is less pronounced in the case of drifts.

1 Introduction

The ground-based total column ozone data set is based on Dobson and Brewer spectrophotometer and filter ozonometer observations available from the *World Ozone and UV Data Centre* (WOUDC) (http://www.woudc.org/). Large longitudinal inhomogeneities in the global ozone distribution and limited spatial coverage of the ground-based network make it difficult to estimate zonal and global total ozone values from station observations directly (Fioletov et al., 2002). The Total Column Ozone (TCO) data set is comprised of the ozone observations from the set ground-based stations worldwide. Most of those stations are located on land in the Northern Hemisphere, and relatively few stations are over the Southern Hemisphere and oceans. Therefore the spatial distribution of ground-based stations is highly irregular. In addition, durations of operations for each station are different. One of the major difficulties in assessing long-

AMTD
8, 3967–4009, 2015

term global total ozone variations is thus data inhomogeneity. Indeed recalibration of ground-based instruments, or interruptions in observation records result in data sets which may have systematic errors that change with time (Fioletov et al., 2002, 2008).

The TCO data set and corresponding satellite measurements has also been widely discussed in the statistics literature. Some authors have noticed *space–time asymmetry* in ozone data (Stein, 2005, 2007; Jun and Stein, 2007, 2008). The other important feature of TCO data is that the spatial dependence of ozone distributions varies strongly with latitude and weakly with longitude, so that homogeneous models (invariant to all rotations) are clearly unsuitable (Stein, 2007). This is why Jun and Stein (2007) assume that the spatial process driving the TCO data is an *axially symmetric* process whose first two moments are invariant to rotations about the Earth's axis, and constructed space–time covariance functions on the sphere × time that are weakly stationary with respect to longitude and time for fixed values of latitude. Jun and Stein (2008) further used linear combinations of Legendre polynomials to represent the coefficients of partial differential operators in the covariance functions. These covariance functions produce covariance matrices that are neither of low rank nor sparse for irregularly distributed observations, as it is the case with ground-based stations. Hence, likelihood calculations can thus be difficult in that situation, and we will not follow this approach.

The aim of this article is to apply a new technique, the stochastic partial differential equation (SPDE) approach in spatial statistics (Lindgren et al., 2010) in order to best evaluate total column ozone spatially from ground based stations. The SPDE approach has already been applied to regularly spaced ozone satellite data by Bolin and Lindgren (2011) but not to ground-level stations, where gains in accuracy are potentially larger due to the gaps in coverage. Furthermore, we quantify the impact of the improvement of these spatial estimations on the computations of time series over various regions. Finally, the SPDE and kriging methods are also used to calculate monthly zonal mean total ozone values and compare them with zonal means calculated from ground-based data and available from the WOUDC (Bojkov and Fioletov, 1995; Fioletov et al., 2002).

AMTD
8, 3967–4009, 2015

Section 2 gives a brief introduction to the theoretical framework of the SPDE technique, a basic description of the universal kriging, and related model selection and diagnostic techniques. Section 3 describes the spatial analysis using TCO data from WOUDC at monthly, seasonal and annual bases. Furthermore, the estimated results of SPDE and kriging are compared with the Total Ozone Mapping Spectrometer (TOMS) satellite data, to examine which method yields approximations closer to satellite data. Finally, the long-term zonal mean trends enable us to conduct a sensitivity analysis by removing stations at random and by introducing long-term drifts at some ground-based stations.

2 Methods

Our main problem is to estimate ozone values at places where it is not observed. Models in spatial statistics that enable this task are usually specified through the covariance function of the latent field. Indeed, in order to assess uncertainties in the spatial interpolation with global coverage, we cannot build models only for the discretely located observations, we need to build an approximation of the entire underlying stochastic process defined on the sphere. Statistical models assumes that the unknown function is a realization of a Gaussian random spatial process. The standard fitting approach, kriging, spatially interpolates values as linear combinations of the original observations, and this constitutes the spatial predictor (with a mean field often estimated as well). Not only large data sets can be computationally demanding for kriging, but kriging struggles to take into consideration nonstationarity (i.e. when physical spatial correlations are different across regions), due to the fixed underlying covariance structure. Recently, a different computational approach (for identical underlying spatial covariance models) was introduced by Lindgren et al. (2010), in which random fields are expressed as a weak solution to a stochastic partial differential equation (SPDE), with explicit links between the parameters of the SPDE and the covariance structure. This approach can deal with large spatial data sets and naturally account for nonstationarity. We review below some

AMTD
8, 3967–4009, 2015

of the recent development on the covariance structure modelling on the sphere, with a particular focus on SPDE and kriging. Computational implementations of SPDE and kriging, with mathematical details, are relegated to Appendix A.

The Matérn covariance function is the most advanced covariance structure used to model dependence of spatial data on the plane. On the sphere, Guinness and Fuentes (2013) show that the kriging prediction using the Matérn function with chordal distance outperform all other types of covariance functions, both in terms of accuracy and quantification of uncertainty. The shape parameter ν, scale parameter κ, and the marginal precision τ^2, parameterize it:

$$C(\boldsymbol{h}) = \frac{2^{1-\nu}}{(4\pi)^{d/2}\Gamma(\nu + d/2)\kappa^{2\nu}\tau^2}(\kappa\|\boldsymbol{h}\|)^{\nu}K_{\nu}(\kappa\|\boldsymbol{h}\|), \quad (1)$$

where $\boldsymbol{h} \in \mathbb{R}^d$ denotes the difference between any two locations $\boldsymbol{s}$ and $\boldsymbol{s}'$: $\boldsymbol{h} = \boldsymbol{s} - \boldsymbol{s}'$, and K_{ν} is a modified Bessel function of the second kind of order $\nu > 0$.

2.1 SPDE approach

Let $X(\mathbf{s})$ be the latent field of ozone measurements $Y(\mathbf{s})$ under observation errors $\epsilon(\mathbf{s})$. Lindgren et al. (2010) use the fact that a random process $X(\mathbf{s})$ on $\mathbb{R}^d$ with a Matérn covariance function (Eq. 1) is the stationary solution to the SPDE:

$$(\kappa^2 - \Delta)^{\alpha/2}\tau X(\mathbf{s}) = \mathcal{W}(\mathbf{s}), \quad (2)$$

where $\mathcal{W}(\mathbf{s})$ is Gaussian white noise, and Δ is the Laplace operator. The regularity (or smoothness) parameter ν essentially determines the order of differentiability of the fields. The link between the Matérn covariance (Eq. 1) and the SPDE formulation (Eq. 2) is given by $\alpha = \nu + d/2$, which makes explicit the relationship between dimension and regularity for fixed α. Unlike kriging, the SPDE approach can be easily manipulated on manifolds. On more general manifolds than $\mathbb{R}^d$, the direct Matérn representation is

AMTD
8, 3967–4009, 2015

not easy to implement, but the SPDE formulation provides a natural generalisation, and the ν parameter will keep its meaning as the quantitative measure of regularity. Instead of defining Matérn fields by the covariance function on these manifolds, Lindgren et al. (2010) used the solution of the SPDE as a definition, and it is much easier and flexible to do so. This definition is valid not only on $\mathbb{R}^d$ but also on general smooth manifolds, such as the sphere. The SPDE approach allows κ and τ to varies with location:

$$(\kappa^2(\mathbf{s}) - \Delta)^{\alpha/2}\tau(\mathbf{s})X(\mathbf{s}) = \mathcal{W}(\mathbf{s}), \tag{3}$$

where $\kappa(\mathbf{s})$ and $\tau(\mathbf{s})$ are estimated by expanding them in a basis of a function space such as the spherical harmonic basis. We estimate the SPDE approach parameters and supply uncertainty information about the surfaces by using the *integrated nested Laplacian approximations* (INLA) framework, available as an R package (http://www.r-inla.org/). For latent Gaussian Markov random fields used to efficiently solve SPDEs on triangulations, INLA provides good approximations of posterior densities at a fraction of the cost of Markov Chain Monte Carlo (MCMC). Note that for models with Gaussian data, the calculated densities are for practical purposes exact.

2.2 Spatial kriging

For locations on spherical domain, $\mathbf{s}_i = (\mathbf{L}_i, \mathbf{l}_i)$, let $Y(\mathbf{s}_i)$ denotes the ozone measured at station i, then the kriging representation can be assumed additive with a polynomial model for the spatial trend (universal kriging):

$$Y(\mathbf{s}_i) = X(\mathbf{s}_i) + e_i = P(\mathbf{s}_i) + Z(\mathbf{s}_i) + e_i,$$

where P is a polynomial which is the fixed part of the model, Z is a zero mean, Gaussian stochastic process with an unknown covariance function K, and e_i are i.i.d. normal errors. The estimated latent field $X(\mathbf{s})$ is then the best linear unbiased estimator (BLUE) of $P(\mathbf{s}) + Z(\mathbf{s})$ given the observed data.

For kriging, the hurdle that we are facing is that we have to define a valid (but flexible enough) covariance model, and furthermore, compared to data on the plane, we must

AMTD
8, 3967–4009, 2015

employ a distance on the sphere. Two distances are commonly be considered. The chordal distance between the two points $(\mathbf{L}_1, \mathbf{l}_1)$ and $(\mathbf{L}_2, \mathbf{l}_2)$ on the sphere is given by

$$\mathrm{ch}(\mathbf{L}_1, \mathbf{L}_2, \mathbf{l}_1 - \mathbf{l}_2) = 2r\left(\sin^2\left(\frac{\mathbf{L}_1 - \mathbf{L}_2}{2}\right) + \cos\mathbf{L}_1 \cos\mathbf{L}_2 \sin^2\left(\frac{\mathbf{l}_1 - \mathbf{l}_2}{2}\right)\right)^{1/2},$$

where r denote the Earth's radius. The more physically intuitive great circle distance between the two locations is $\mathrm{gc}(\mathbf{L}_1, \mathbf{L}_2, \mathbf{l}_1 - \mathbf{l}_2) = 2r \arcsin\{ch(\mathbf{L}_1, \mathbf{L}_2, \mathbf{l}_1 - \mathbf{l}_2)\}$. However, Gneiting (2013) pointed out that using the great circle distance in the original Matérn covariance function (Eq. 1) would not work, as it may not yield a valid positive definite covariance function. Therefore in this study we use the chordal distance in kriging. The main advantage of using the chordal distance is that it is well defined on spherical domain, as it restricts positive definite covariance functions on $\mathbb{R}^3$ to $\mathbb{S}^2$ (Jun and Stein, 2007). For the ozone data, we specify the Matérn covariance function defined in Eq. (1) in the kriging approach in order to compare the performance with the SPDE approach for exactly the same covariance function. The relevant model diagnostic and selection criteria are described in Appendix B. Note that the smoothness parameter ν is allowed to be selected in kriging, whereas it is fixed at $\nu = 0.5$ in the SPDE approach.

3 Mapping accuracy

In this section, we produce statistical estimates of monthly ozone maps, using TCO data from WOUDC. We consider TCO data in January 2000 as an illustration, which contains 150 ground-based ozone observations around the world. All ozone values in this article are in Dobson Units (DU). We first choose the model set-ups for both SPDE and kriging below.

With the SPDE approach, as the smoothness parameter ν is through the relationship $\alpha = \nu + d/2$, we only need to choose the basis expansion order to represent κ and τ. To choose the best maximal order of the spherical harmonic basis, we fitted models with different maximal orders of spherical harmonics for the expansions of κ and τ in

AMTD
8, 3967–4009, 2015

order to estimate them thereafter (the default choice in the R-INLA package). The best fitted model is for a spherical harmonics basis with maximal order 3 since it yielded the lowest Generalized Cross Validation (GCV) SD computed in Eq. (B2), which yield a total of 9 parameters to be estimated (4 parameters for the expansions of κ and τ, and 1 parameter for the variance). For kriging, we need to choose the smoothness parameter in the Matérn covariance function before estimating the univariate quantities κ and τ^2. The same GCV SD criterion is used to evaluate the model performance. The smoothing parameter $\nu = 20$ minimizes the σ_{GCV} for these ozone data.

To compare the performance of the SPDE approach with kriging, the same σ_{GCV} criterion is used as it balances well predictive power v. overfitting across methods. Figure 1 shows the predicted mean and SD ozone maps on January 2000. The spatial distributions of ozone means are similar for SPDE and kriging in the Northern Hemisphere, but there are differences in the Southern Hemisphere. These differences arise from the asymmetry of available stations in the two hemispheres. The spatial distributions of the SD present similar general patterns for the two techniques. The uncertainties are higher where with fewer station available, see the large uncertainty distribution at the South Pacific Ocean. SD of SPDE predictions are much smaller than the SD of the kriging predictions, especially where fewer observations are available (e.g. mid-Atlantic, and South Pacific), but are larger near the North Pole; this maybe due to kriging underestimating its own uncertainty.

In order to achieve a better estimation, the monthly mean "norms" (Bojkov and Fioletov, 1995) (or total ozone "climatology") are calculated for each station and each month of the year over the whole period and then subtracted from the data. The norms are used as a first approximations to remove the general spatial trend. For each station for each month, spatial interpolation through SPDE and kriging were performed to these deviations.

We now start an illustration to 6 years of monthly observations. The results of the analysis of ozone data averaged from 2000 to 2005 are shown in Table 1. The averaged number of available stations is denoted by $\overline{n}$, and RSS indicates residuals sum of

AMTD
8, 3967–4009, 2015

square, which is defined in Eq. (B1). The SPDE approach provides a better fit than the kriging for all months. The effective degree of freedom n_{eff} is higher in the SPDE approach as it is more complex than kriging. Higher effective degrees of freedom means smaller values in the σ_{GCV} denominator ($n - n_{\text{eff}}$) thus higher values for σ_{GCV} to account for overparametrization. Nevertheless, σ_{GCV} values for the SPDE approach are still all much lower than for kriging in all cases. This means that the residuals sum of squares (RSS) in SPDE approach is drastically smaller than the residuals sum of squares for kriging. Thus the SPDE approach supplies a much better fit to the true ozone observation.

Table 1 also reports regional RSSs by dividing the Earth into the Northern Hemisphere ($> 30^\circ$ N), Tropics (30° S–30° N) and Southern Hemisphere ($< 30^\circ$ S). In general, over half of the ground-based stations are located on the Northern Hemisphere, which gives rise to higher RSS with respect to other regions as the RSSs are not normalized by the number of observations. RSSs estimated by SPDE and kriging show similar patterns across months, and across regions. Lower estimation errors can be found in September–November and higher errors occur in March–May. The ratio of RSS between kriging and SPDE (Relative RSS or RR) are displayed in the table. The SPDE method always improves upon kriging, with the highest improvements being in October in the Southern Hemisphere (a very large ratio of 9.45).

3.1 Seasonal and annual effects

Seasonal ozone data are obtained by averaging the corresponding monthly data (but all months of every season must be available to create such seasonal averages). Table 2 shows the seasonal results over year 2000–2005. The SPDE approach and kriging reveal different seasonal effects in RSSs. Their respective highest errors are in December-January-February (DJF) for spatial kirging and in June-July-August (JJA) for SPDE. Moreover, the values of σ_{GCV} and RSS from this seasonal analysis are smaller than the corresponding analysis for each month of the associated season, both in SPDE approach and kriging, and are also closer across the two competing

AMTD
8, 3967–4009, 2015

techniques due to additional averaging smoothing out the gains in accuracy. Nevertheless the SPDE approach still provides a better fit than kriging in all seasons. Figure 2 and 3 shows the seasonal ozone maps of means and SD, respectively. The maps for SD again reveal the higher estimated error in regions without stations. Again, higher RSSs for kriging may reveals some underestimation of the uncertainties.

The annual ozone data is obtained by creating an annual average, which also means that stations with record interruptions are not used. Therefore less stations are available for this exercise. To see the improvement of the annual based analysis over seasonally and monthly analyses, Table 3 shows the annual averaged results by month and seasonally, and results directly obtained by doing the analysis on the annual mean. Although there are less stations in annual-based and seasonal-based data than in monthly data, the errors are lower than for monthly data over the years both in SPDE and kriging, and the results directly obtained from annual means yields even lower RSS and σ_{GCV} than the results averaged by seasons due to smooth variation.

3.2 Comparison with satellite data

In this section, we assess the match between satellite observations and spatial predictions based on ground-level stations. The Total Ozone Mapping Spectrometer (TOMS) data on monthly averages are obtained from the NASA website (http://ozoneaq.gsfc.nasa.gov/), where we collected the Earth Probe (25 July 1996–31 December 2005) satellite data with grid $1^{\circ} \times 1.25^{\circ}$. We calculate the differences over all grid cells and summarize it by the root mean square error (RMSE). Let $\hat{y}_i$ be the estimated result from the SPDE or kriging on grid i, and y_i^{s} denotes the satellite value on grid i, then the (normalized) RMSE is given by

$$\mathrm{RMSE} = \sqrt{\frac{\sum_{i=1}^{n} \left(\hat{y}_i - y_i^{\mathrm{s}}\right)^2}{n}},$$

where $n = 180 \times 288$ is total number of grid cells. However, satellite data are unavailable over high latitudes in DJF and MAM (March-April-May), and over low latitudes in JJA

AMTD
8, 3967–4009, 2015

and SON (September-October-November). Therefore we restrict the calculations of RMSEs between 60° S–60° N.

Monthly comparisons over 2000–2005 are shown in Table 4. Ozone surfaces predicted by the SPDE approach are closer to the satellite data than the predictions from kriging over all months. The highest improvement of SPDE over kriging is 69.92 % in October and the lowest is 22.78 % in July. Also, in contrast with relatively unstable monthly predictions by kriging, SPDE shows more consistency in predictions of monthly ozone variations.

Figures 4 and 5 map the differences of surface predictions of kriging and SPDE methods with respect to satellite data over 60° S–60° N on January, April, July and October 2000. The differences in October turn out to be much larger than in other months, therefore a different scale is used. These maps indicate the overestimation (red) and underestimation (blue) with respect to satellite data. Similar patterns in deviations are revealed for both techniques, but SPDE displays less magnitude in the deviations than kriging. One noticeable feature is that the pattern of deviation from satellite data is strongly related to the distribution of ground based stations: for instance, the kriging predicted surfaces tend to underestimate the values over the South Pacific Ocean, where few stations are available. The surface predictions by SPDE achieve a clear improvement in predictions compared to kriging over areas with less stations, especially on January and October.

The seasonal predicted total ozone is obtained by averaging the corresponding monthly means. We excluded stations that have interruptions in their records. Therefore less observations are used to predict seasonal means. The RMSEs between predicted surface and satellite data are presented in Table 5. In general, seasonal maps should agree better with satellite-based maps than monthly maps. However, less observations are used in seasonal predictions and that may trigger high RMSEs in the kriging estimation in particular. In those circumstances, the SPDE approach shows robustness against observations loss. Figures 6 and 7 show TOMS maps of all seasons in 2000 in top panels, and differences with predictions from SPDE and kriging. Underestima-

AMTD
8, 3967–4009, 2015

tion at the South Pacific are in accordance with expectations for both techniques, but surface predictions by SPDE achieve a better fit than kriging, especially in SON.

4 Impact on long-term changes

In this section, we show how variations in time of the zonal means can be improved by employing the more accurate SPDE-based mapping technique instead of kriging.

4.1 Zonal mean time series analysis

To see how the ozone zonal means change over time over the same stations with different algorithms, we choose the stations which supplied data at least 25 years between 1979 and 2010. Hence 67 stations are used to construct these zonal mean time series. There is a strong asymmetry between the Southern Hemisphere (6 stations) and the Northern Hemisphere (48 stations); 13 stations at the Tropics (defined as 30° S–30° N.) The zonal means were constructed by averaging the estimations obtained from either kriging or SPDE, over a grid of 1° × 1°.

In order to overcome the underestimation over the South Pacific (see Fig. 4) and achieve a better estimation of long-term global zonal means, the monthly mean norms for each station were subtracted from observations over all the period. Then for each month, spatial interpolation through SPDE and kriging were performed to the deviations. The ozone norms were added back to these deviations in order to compare zonal means over the corresponding belts.

In this study, we compare the zonal mean time series estimated by SPDE and kriging with Solar Backscatter Ultraviolet (SBUV) satellite instrument merged ozone data described by Frith et al. (2014) (http://acd-ext.gsfc.nasa.gov/Data_services/merged/) and a dataset based on ground-based data available from the WOUDC (Bojkov and Fioletov, 1995; Fioletov et al., 2002). The SBUV merged satellite data sets incorporated the measurements from eight backscatter ultraviolet instruments (BUV on Nimbus 4, SBUV

AMTD
8, 3967–4009, 2015

on Nimbus 7, and a series of SBUV/2 instruments on NOAA satellites) processed with the v8.6 algorithm (Bhartia et al., 2013). The WOUDC ground-based zonal mean data set is based on the following technique: firstly, monthly means for each point of the globe were estimated from satellite Total Ozone Mapping Spectrometer (TOMS) data for 1978–1989. Then for each station and for each month the deviations from these means were calculated, and the belt's value for a particular month was estimated as a mean of these deviations. The calculations were done for 5-degree broad latitudinal belts. In order to take into account various densities of the network across regions, the deviations of the stations were first averaged over 5 by 30° cells, and then the belt mean was calculated by averaging these first set of averages over the belts. Till this point the data in the different 5° belts were based on different stations (i.e., were considered independent). However, the differences between nearby belts are small. Hence one can reduce the errors of the belt's average estimations without loss of accuracy by using some smoothing or approximation. So the zonal means were then approximated by zonal spherical functions (Legendre polynomials cosine of the latitude) to smooth out spurious variations. Therefore this methodology (Bojkov and Fioletov, 1995) shares some ideas with SPDE in terms of taking advantage of spherical functions for spatial interpolation over the globe, but this methodology can only be conducted on zonal means calculation, rather than global surface prediction. The merged satellite and the WOUDC data sets were compared again recently and demonstrated a good agreement (Chiou et al., 2014).

To investigate the pattern of zonal mean long term changes in detail, Fig. 8 shows the monthly means from SBUV merged data (black), WOUDC dataset (green), kriging (red) and SPDE (blue). Kriging and SPDE estimated means both match well satellite data and the WOUDC dataset in the Northern Hemisphere. Kriging means in the tropics fluctuate heavily and are unrealistic in some years, which indicates that kriging may perform well at some locations but can provide distorted results at other locations; moreover the large kriging-based fluctuations in the beginning of the period may be due to a lack of stations in the early years of 1979–2010. SPDE estimated means are

AMTD
8, 3967–4009, 2015

more robust under this circumstance. Limited stations in the South Hemisphere may trigger underestimation and disappear of estimated annual cycle in SPDE and kriging. Therefore we carry out a seasonal smoothing by averaging September to November to estimate better the annual peak over the Southern Hemisphere (i.e. October). This smoothing algorithm improves the match with SBUV data.

4.2 Sensitivity analysis

The final step is to conduct a sensitivity analysis for the long-term zonal mean estimations against either randomly removed stations, or drifts in some of ground-based observations. To see the impact of removing stations to the long-term ozone zonal mean change, we choose 57 stations (39 stations in the Northern Hemisphere, 10 stations in the Tropics and 8 stations in the Southern Hemisphere) which provided data over the entire period 1990 to 2010. We randomly remove 5, 10, 20 and 30 stations out of these set of stations by taking into account the relative weights of the respective regions, and estimate the zonal mean trends in each case. The stations removed are randomly chosen by the design in Table 6.

Furthermore, to illustrate possible variations in the sensitivity analysis, we randomly draw 5 times stations which need to be removed, labelled cases 1–5. The time series for different zonal mean trends over the latitude band 30–60° N and 30–60° S are displayed in Figs. 9 and 10, respectively. The impact of randomly removing stations in the Northern Hemisphere is small, even in the case of 30 stations removed (over half of the observations). The Southern Hemisphere is more sensitive to loss information because only few stations are located in there. The more stations are removed, the more fluctuations appear in the time series. The main finding is that the long-term effects estimated by SPDE are again more robust than the ones obtained by kriging, especially for the case of 30 stations removed (with only 2 stations left in the SH). The kriging estimated trends can become be chaotic for cases 2 and 4, and under this circumstance the total ozone annual cycle become unidentifiable.

AMTD
8, 3967–4009, 2015

We use case 1 for further illustration, where both kriging and SPDE estimated well with respect to other cases. Figure 11 shows deviations in time series in the annual mean total ozone estimated by SBUV data, WOUDC dataset, SPDE and kriging. We can see that both SPDE and kriging estimate well in the Northern Hemisphere. Kriging prediction underestimate means significantly over the Tropics and the Southern Hemisphere, while SPDE estimated means are close to SBUV trends. In summary, the SPDE approach is more robust than kriging against incomplete information. Note that SPDE estimated trends using all stations are closer to SBUV observations than the WOUDC dataset at the Tropics and Southern Hemisphere overall.

For the second part of sensitivity analysis, we add random long-term drifts into observations due to instrument-related problems. In reality, all observations from a ground-level station are often be biased by 5–10 DU (2–3 %) over a period of several years. For the setting of drifts, let y_{ij} be the ozone observations at station i and time j. We randomly select some stations i and set

$$y^*_{ij} = a_i y_{ij},$$

where $a_i \sim N(1, 0.03^2)$ is the slope over every 5 year periods, i.e., one slope factor for 1990–1994, then different drifts for 1995–1999, 2000–2004 and 2005–2010. This setting means that stations were randomly selected and drift values were then randomly generated, but the drifts are fixed for particular station over every 5 or 6 years.

Using the same 57 stations which provided data consistently over 1990 to 2010, the zonal mean trends were estimated with these added drifts subsets of randomly selected 5, 10, 20 and 30 stations. We consider 5 sets of random drifts as well to account for possible random variations in the selection process. The time series in each case are shown in Figs. 12 and 13 for the Northern and Southern Hemisphere. Kriging estimations hold robust in the case of over half of stations are drifted, SPDE also displays robustness to drift. We use case 1 as further illustration. Figure 14 shows the annual mean total ozone deviations in time series for SBUV, WOUDC dataset,

AMTD
8, 3967–4009, 2015

kriging and SPDE estimated means when drifts are present. SPDE estimated trends reveals to be superior to kriging at the Tropics and Southern Hemisphere overall.

Table 7 reports monthly, seasonal and annual average RMSEs obtained by comparing the WOUDC, SPDE, and kriging estimated zonal means to the SBUV zonal means over 1990–2010. We can see that SPDE is always superior to kriging. Furthermore, SPDE zonal means are closer to satellite zonal means than WOUDC zonal means for annual and seasonal averages in the Northern Hemisphere, despite using less stations (39) than WOUDC that uses all available stations each month. It shows the superior ability of SPDE to interpolate variations over the globe than WOUDC. However, for monthly zonal means, SPDE zonal means are further away from satellite zonal means than WOUDC zonal means. Indeed, there is much less averaging over one month, and the SPDE approach can suffer from the lack of stations at some locations to describe particular monthly features that can be more pronounced than seasonal or annual averages. SPDE zonal means over the Tropics and Southern Hemisphere in monthly and seasonal analysis suffer greatly as only 10 stations are used in the Tropics and 8 in the Southern Hemisphere (whereas WOUDC can use up to 20–30 in the Southern Hemisphere). We expect that for operational purposes, using all the available stations (usually around 130–150 as seen in Table 3, not 57 as done here for convenience) for each month would allow SPDE to clearly outperform WOUDC everywhere at all frequencies, as it does already with less stations in the Northern Hemisphere for annual and seasonal averages. Such a data set would constitute a improvement for the study of trends based on ground level instruments.

5 Conclusions

In summary, the kriging method may perform fairly well in global behavior, but displays misfit locally. The misfits will be averaged out when zonal means are estimated, but it reveals the relatively higher errors in estimations compared to the SPDE spatial prediction method for mapping. Moreover, both the estimation uncertainty of kriging and

AMTD
8, 3967–4009, 2015

SPDE methods considerably depend on the location of stations, but the SPDE approach outperforms kriging in terms of the uncertainty quantification in areas with few stations. The time series analysis in the Northern Hemisphere are relatively better than the Southern Hemisphere as there is a much denser network of stations than in the Southern Hemisphere. The sensitivity analysis suggests that the ground-based network can provide a reliable source of data for estimation of the long-term ozone trends. In the Northern Hemisphere, annual means can be successfully estimated even if half of the available sites is excluded from the analysis. This is not the case for the Tropical belt and Southern Hemisphere where the number of sites is very limited. Additional 3 % biases over 5 year intervals at up to the half of the network have relatively small impact on the estimated zonal means. This suggest that the network can tolerate some systematic errors as long as instruments are calibrated on a regular basis (5 years in our tests) that remove such biases. Overall, when stations are removed or drift, the SPDE approach shows more robustness than kriging, and thus, for current observations, should be a preferred method.

Appendix A: Computational details of kriging and SPDE approaches

A1 SPDE approach

The algorithm of estimation of parameters in SPDE works as follows. Let $Y(\mathbf{s})$ be an observation of the latent field $X(\mathbf{s})$, the model is given by

$$Y(\mathbf{s}) = X(\mathbf{s}) + \epsilon(\mathbf{s}),$$

where $X(\mathbf{s})$ is the solution of the SPDE approach (Eq. 3), and observation error $\epsilon(\mathbf{s})$ is zero mean Gaussian noise with variance σ^2. This latent field can be built on a basis representation

$$x(\mathbf{s}) = \sum_{k=1}^{n} \psi_k(\mathbf{s}) w_k,$$

AMTD
8, 3967–4009, 2015

where the w_k's are stochastical weights which are chosen so that the $x(\mathbf{s})$ approximates the distribution of solutions to the SPDE on the sphere. The basis functions $\psi_k(\mathbf{s})$'s are chosen by a Finite Element Method in order to obtain a Markov structure, and to preserve it when conditioning on local observations. To allow an explicit expression of the precision matrix for the stochastical weights, we use a piecewise linear basis functions defined by a triangulation on the sphere. Let $\mathbf{C} = \langle \psi_i, \psi_j \rangle$ and $\mathbf{G} = \langle \nabla\psi_i, \nabla\psi_j \rangle$ be matrices used in the construction of the Finite Element solutions of SPDE approach. Then in case of $\alpha = 2$, the precision matrix for the weights $\{w_i\}$ is given by

$$\mathbf{Q} = \tau^2(\kappa^4\mathbf{C} + 2\kappa^2\mathbf{G} + \mathbf{G}\mathbf{C}^{-1}\mathbf{G})$$

the elements of $\mathbf{Q}$ have explicit expressions as functions of κ^2 and τ (Lindgren et al., 2010).

As pointed out in Jun and Stein (2008), the spatial mean structure on a sphere can be modelled using a regression basis of spherical harmonics; however, since the data set only contains measurements from one specific event, it is not possible to identify which part of the variation in the data come from a varying mean and which part that can be explained by the variance–covariance structure of the latent field. To avoid this identifiability problem. The parameter $\kappa(\mathbf{s})$ and $\tau(\mathbf{s})$ must be positive, and their logarithm can be decomposed as

$$\log\kappa(\mathbf{s}) = \sum_{k,m} \kappa_{k,m} S_{k,m}(\mathbf{s})$$

$$\log\tau(\mathbf{s}) = \sum_{k,m} \tau_{k,m} S_{k,m}(\mathbf{s})$$

AMTD
8, 3967–4009, 2015

where $S_{k,m}$ is the spherical harmonic of order k and mode m. The real spherical harmonic $S_{k,m}(s)$ of order $k \in \mathbb{N}_0$ and mode $m = -k, \ldots, k$ is defined as

$$S_{k,m}(s) = \sqrt{\frac{2k+1}{4\pi}\frac{(k-|m|)!}{(k+|m|)!}} \begin{cases} \sqrt{2}\sin(ml)P_{k,|m|}(\sin L) & \text{if } -k \le m < 0, \\ P_{k,0}(\sin L) & \text{if } m = 0, \\ \sqrt{2}\cos(ml)P_{k,m}(\sin L) & \text{if } 0 < m \le k, \end{cases}$$

where $P_{k,m}$ are associated Legendre polynomials:

$$P_{k,m}(x) = (-1)^m(1-x^2)^{m/2}\frac{d^m}{dx^m}P_k(x),$$

where P_k are Legendre polynomials:

$$P_k(x) = \frac{1}{2^k k!}\frac{d^k}{dx^k}(x^2-1)^k,$$

Regarding the computational implementation of the SPDE approach, one common choice would be to use a Metropolis–Hastings algorithm, which is easy to implement, but computationally inefficient (Bolin and Lindgren, 2011). A better way is to use direct numerical optimization to estimate the parameters by employing *integrated nested Laplace approximations* (INLA) framework, available as an R package (http://www.r-inla.org/). For latent Gaussian Markov random fields, INLA provides good approximations to posterior densities at a fraction of the cost of MCMC. For models with Gaussian data, the calculated densities are for practical purposes exact. The main limitation is that R-INLA provides $0 < \alpha \le 2$ case (though $0 < \alpha < 2$ not as extensively tested). So with $\alpha = 2$ and three dimensions, the smoothness parameter ν must be fixed at 0.5 due to the relationship $\alpha = \nu + d/2$.

A2 Spatial kriging

For the ozone data, we specified a second order linear polynomial for $P(\mathbf{s})$ and a mean zero, Gaussian stochastic process with a Matérn covariance function for $Z(\mathbf{s})$ defined

AMTD
8, 3967–4009, 2015

in Eq. (1) and used chordal distance as spherical metric. We implemented kriging with the R package *fields*. We also estimated the smoothness parameter ν as it is not fixed for the kriging approach.

Appendix B: Model diagnostic and selection

To assess the performance of model fitting, the residuals are considered. Raw residuals are defined as the difference of the observed values and fitted values. They can be interpreted as estimators of the errors e_i (and are denoted by $\hat{e}_i$). Therefore the performance of model fitting can be assessed by the residual sum of square (RSS):

$$\mathrm{RSS} = \sum_{i=1}^{n} \hat{e}_i^2. \tag{B1}$$

Furthermore, to choose the number of basis functions for the smoothing parameter and to compare the performance of SPDE approach and kriginqg, we also used the generalised cross validation (GCV) criterion for comparing different models (Wahba, 1985). Let $\hat{y}$ be the predictor vector for the observed y with $\hat{y} = A(\lambda)y$, where A is the $n \times n$ smoothing matrix, and let the $n_{\mathrm{eff}} = \mathrm{tr}A(\lambda)$ measure the effective number of degrees of freedom attributed to the smooth surface, which is also called the effective number of parameter. The GCV criterion selects λ as the minimizer of the GCV function:

$$V(\lambda) = \frac{n^{-1}\|(I - A(\lambda)y)\|}{[n^{-1}\mathrm{tr}(I - A(\lambda))]^2} = \frac{1}{n}\sum_{i=1}^{n}\left(\frac{y_i - \hat{y}_i}{1 - \mathrm{tr}(A(\lambda))/n}\right)^2$$

An alternative frequentist estimate for the residual variance, σ^2_{GCV}, is defined by

$$\sigma^2_{\mathrm{GCV}} = \frac{\sum_{i=i}^{n}(y_i - \hat{y}_i)^2}{n - \mathrm{tr}(A(\lambda))}. \tag{B2}$$

AMTD
8, 3967–4009, 2015

The GCV in its standard form finds the weighted residual sum of squares when each data point (i.e. station) is omitted and predicted from the remaining points. The weights depend on the variance of the measurement error and the location of each point. The σ_{GCV} measures the residual variance but mitigates the effect of the number of parameters used in the model.

Acknowledgements. Kai-Lan Chang was supported by the Taiwanese government sponsorship for PhD overseas study. S. Guillas was partially supported by a Leverhulme Trust research fellowship on "stratospheric ozone and climate change" (RF/9/RFG/2010/0427). We also thank the NOAA Atmospheric Composition and Climate program as the source of funding for this paper.

References

Bhartia, P. K., McPeters, R. D., Flynn, L. E., Taylor, S., Kramarova, N. A., Frith, S., Fisher, B., and DeLand, M.: Solar Backscatter UV (SBUV) total ozone and profile algorithm, Atmos. Meas. Tech., 6, 2533–2548, doi:10.5194/amt-6-2533-2013, 2013. 3979

Bojkov, R. D. and Fioletov, V. E.: Estimating the global ozone characteristics during the last 30 years, J. Geophys. Res.-Atmos., 100, 16537–16551, doi:10.1029/95JD00692, 1995. 3969, 3974, 3978, 3979

Bolin, D. and Lindgren, F.: Spatial models generated by nested stochastic partial differential equations, with an application to global ozone mapping, Ann. Appl. Stat., 5, 523–550, doi:10.1214/10-AOAS383, 2011. 3969, 3985

Chiou, E. W., Bhartia, P. K., McPeters, R. D., Loyola, D. G., Coldewey-Egbers, M., Fioletov, V. E., Van Roozendael, M., Spurr, R., Lerot, C., and Frith, S. M.: Comparison of profile total ozone from SBUV (v8.6) with GOME-type and ground-based total ozone for a 16-year period (1996 to 2011), Atmos. Meas. Tech., 7, 1681–1692, doi:10.5194/amt-7-1681-2014, 2014. 3979

Fioletov, V. E., Labow, G., Evans, R., Hare, E., Köhler, U., McElroy, C., Miyagawa, K., Redondas, A., Savastiouk, V., Shalamyansky, A., Staehelin, J., Vanicek, K., Weber, M.: Performance of the ground-based total ozone network assessed using satellite data, J. Geophys. Res.-Atmos., 113, 2008. 3969

AMTD
8, 3967–4009, 2015

Fioletov, V. E., Bodeker, G. E., Miller, A. J., McPeters, R. D., and Stolarski, R.: Global and zonal total ozone variations estimated from ground-based and satellite measurements: 1964–2000, J. Geophys. Res., 107, D22, ACH 21-1–ACH 21-14 doi:10.1029/2001JD001350, 2002. 3968, 3969, 3978

Frith, S. M., Kramarova, N. A., Stolarski, R. S., McPeters, R. D., Bhartia, P. K., and Labow, G. J.: Recent changes in column ozone based on the SBUV version 8.6 merged ozone dataset, J. Geophys. Res., 119, 16, 9735–9751, doi:10.1002/2014JD021889, 2014. 3978

Gneiting, T.: Strictly and non-strictly positive definite functions on spheres, Bernoulli, 19, 1327–1349, doi:10.3150/12-BEJSP06, 2013. 3973

Guinness, J. and Fuentes, M.: Covariance functions for mean square differentiable processes on spheres, submitted, 2013. 3971

Jun, M. and Stein, M. L.: An approach to producing space-time covariance functions on spheres, Technometrics, 49, 468–479, doi:10.1198/004017007000000155, 2007. 3969, 3973

Jun, M. and Stein, M. L.: Nonstationary covariance models for global data, Ann. Appl. Stat., 2, 1271–1289, doi:10.1214/08-AOAS183, 2008. 3969, 3984

Lindgren, F., Rue, H., and Lindström, J.: An explicit link between Gaussian fields and Gaussian Markov random fields: the stochastic partial differential equation approach, J. Roy. Stat. Soc. B, 73, 423–498, doi:10.1111/j.1467-9868.2011.00777.x, 2010. 3969, 3970, 3971, 3972, 3984

Stein, M. L.: Space-time covariance functions, J. Am. Stat. Assoc., 100, 310–321, doi:10.1198/016214504000000854, 2005. 3969

Stein, M. L.: Spatial variation of doi:10.1214/07-AOAS106, 2007. 3969

Wahba, G.: A comparison of GCV and GML for choosing the smoothing parameter in the generalized spline smoothing problem, Ann. Stat., 13, 1378–1402, 1985. 3986

AMTD
8, 3967–4009, 2015

Table 1. Comparison of the generalised cross validation error (σ_{GCV}) and the residual sum of square (RSS) and relative RSS (RR) for kriging (K) and SPDE (S) model averaged of 2000–2005 by month. Estimation is reported by Northern Hemisphere (NH), Tropic and Southern Hemisphere (SH).

Global		Jan	Feb	Mar	Apr	May	Jun	Jul	Aug	Sep	Oct	Nov	Dec
Kriging	$\overline{n}$	135.33	144.33	146.17	146.00	142.50	143.33	143.00	145.33	146.00	142.67	140.17	129.50
	n_{eff}	16.89	25.69	30.51	19.57	24.14	15.46	14.39	29.63	36.93	38.24	28.86	20.67
	σ_{GCV}	15.10	14.05	12.11	12.45	10.33	10.54	9.87	9.75	9.68	9.53	12.35	12.71
	RSS	28 535	25 611	18 323	20 711	13 258	14 770	12 637	11 479	10 654	9645	17 550	19 129
SPDE	n_{eff}	70.68	59.76	69.47	50.27	65.99 7	57.25	38.93	52.22	52.04	54.84	66.78	60.54
	σ_{GCV}	8.43	9.81	7.98	10.00	7.21	8.01	8.44	7.89	7.72	7.00	8.71	7.93
	RSS	6477	8873	5768	11 728	4660	6761	7802	6779	7055	5030	6198	4928
	RR	4.41	2.82	3.00	1.77	2.84	2.18	1.62	1.69	1.51	1.92	2.83	3.88
Region RSS		Jan	Feb	Mar	Apr	May	Jun	Jul	Aug	Sep	Oct	Nov	Dec
NH	$\overline{n}$	89.50	98.50	101.67	104.00	102.50	103.83	103.00	103.00	102.67	98.50	95.50	84.67
	K	26 035	22 234	15 507	16 144	10 498	11 288	8435	7238	7179	6748	13 035	16 690
	S	5066	6837	4369	9148	3721	5539	5702	5440	6019	4279	4693	3379
	RR	5.14	3.25	3.55	1.76	2.82	2.04	1.48	1.33	1.19	1.58	2.78	4.94
Tropic	$\overline{n}$	27.83	27.33	26.33	26.33	26.50	26.67	27.33	27.33	26.83	26.67	27.00	27.17
	K	1778	2182	2120	2988	1254	1632	2264	1228	957	1042	1360	1411
	S	730	1020	845	1609	575	780	1605	849	665	554	995	1012
	RR	2.44	2.14	2.51	1.86	2.18	2.09	1.41	1.45	1.44	1.88	1.37	1.39
SH	$\overline{n}$	18.00	18.50	18.17	15.67	13.50	12.83	12.67	15.00	16.50	17.50	17.67	17.67
	K	722	1195	696	1580	1505	1850	1938	3012	2518	1855	3155	1028
	S	682	1016	553	971	364	443	495	490	372	196	510	536
	RR	1.06	1.17	1.26	1.63	4.13	4.18	3.92	6.15	6.78	9.45	6.19	1.92

AMTD
8, 3967–4009, 2015

Table 2. Comparison of the generalised cross validation error (σ_{GCV}) and residual sum of square (RSS) for kriging and SPDE approach averaged of years 2000–2005 by season.

	Season	DJF	MAM	JJA	SON	Average
	$\overline{n}$	117.17	132.83	132.17	130.67	128.21
Kriging	n_{eff}	18.73	20.68	11.53	32.77	20.93
	σ_{GCV}	9.47	9.20	8.39	8.19	8.81
	RSS	10 274	9990	8526	6783	8893
SPDE	n_{eff}	51.71	59.70	29.12	68.32	52.21
	σ_{GCV}	7.02	6.55	7.52	5.95	6.76
	RSS	3847	3833	6147	2724	4138

AMTD
8, 3967–4009, 2015

Table 3. Comparison of the generalised cross validation error (σ_{GCV}) and residual sum of square (RSS) for kriging and SPDE approach of years 2000–2005. The monthly and seasonally results are averaged over each year, and annual results are directly estimated by annual means from each station.

		Year	2000	2001	2002	2003	2004	2005
Monthly		$\overline{n}$	143.25	151.58	147.50	136.17	135.25	138.42
	Kriging	n_{eff}	30.95	17.88	30.82	24.52	20.51	25.81
		σ_{GCV}	10.85	12.60	10.34	10.98	12.75	11.72
		RSS	14 473	23 946	12 693	13 930	20 112	15 998
	SPDE	n_{eff}	63.09	41.46	68.70	67.94	56.55	51.64
		σ_{GCV}	7.31	10.29	6.95	7.33	8.75	8.94
		RSS	4977	13 361	4063	3902	7390	7337
Seasonally		$\overline{n}$	126.00	135.75	135.50	123.75	120.50	127.75
	Kriging	n_{eff}	28.05	12.48	24.69	21.11	18.43	20.82
		σ_{GCV}	8.18	10.38	7.71	8.37	8.63	9.63
		RSS	6533	15 281	6552	7299	7781	9912
	SPDE	n_{eff}	57.14	42.38	57.52	65.85	48.06	42.31
		σ_{GCV}	5.99	8.47	6.00	5.59	6.67	7.84
		RSS	2583	7951	3148	1941	3797	5406
Annually		n	83	97	101	90	87	97
	Kriging	n_{eff}	24.10	23.67	11.21	8.35	12.65	12.70
		σ_{GCV}	5.05	5.34	6.29	7.23	5.95	8.67
		RSS	1501	2094	3553	4271	2629	6343
	SPDE	n_{eff}	48.93	41.61	30.72	49.93	31.97	22.91
		σ_{GCV}	3.13	3.70	5.17	5.28	4.74	6.49
		RSS	367	982	2092	1059	1345	4372

AMTD
8, 3967–4009, 2015

Table 4. Comparison of RMSEs for kriging and SPDE approach predictions with satellite data over all months and averaged from 2000 to 2005.

Month	Jan	Feb	Mar	Apr	May	Jun	Jul	Aug	Sep	Oct	Nov	Dec	AVE.
Kriging	19.82	25.20	21.62	17.37	26.83	15.52	13.26	32.99	48.99	51.14	39.02	28.70	28.37
SPDE	12.82	11.00	12.90	12.40	20.54	11.17	10.24	21.83	16.17	15.54	13.95	18.18	14.73
percentage of improvement	35.32	56.34	40.34	28.63	23.46	28.00	22.78	33.83	67.00	69.62	64.25	36.68	48.09

AMTD
8, 3967–4009, 2015

Table 5. Comparison of RMSEs for kriging and SPDE approach predictions with satellite data over all seasons and averaged from 2000 to 2005.

Season	DJF	MAM	JJA	SON	Average
Kriging	20.19	19.52	15.46	43.57	24.69
SPDE	14.05	16.11	12.17	14.41	14.19
percentage of improvement	30.38	17.48	21.29	66.93	42.53

AMTD
8, 3967–4009, 2015

Table 6. Design of the sensitivity analysis: stations to be removed are randomly selected within each region.

Number of removed	5	10	20	30	Total
NH (90–30° N)	3	6	12	18	39
Tropic (30° S–30° N)	1	2	4	6	10
SH (30–90° S)	1	2	4	6	8

AMTD
8, 3967–4009, 2015

Table 7. RMSEs of annual, seasonal and monthly total mean ozone from WOUDC dataset, SPDE and kriging estimated means (using 57 stations) against SBUV data over 1990–2010.

	Annual			Seasonal			Monthly		
	WOUDC	SPDE	Kriging	WOUDC	SPDE	Kriging	WOUDC	SPDE	Kriging
NH	3.17	2.37	2.94	3.40	3.21	3.54	3.95	4.21	4.40
Tropic	2.07	4.01	9.59	2.42	5.22	10.47	2.56	5.79	10.66
SH	4.51	3.96	8.39	4.39	8.84	15.33	6.10	11.07	15.58
Global	2.28	2.36	6.85	2.55	3.55	8.91	2.92	4.60	9.03

AMTD
8, 3967–4009, 2015

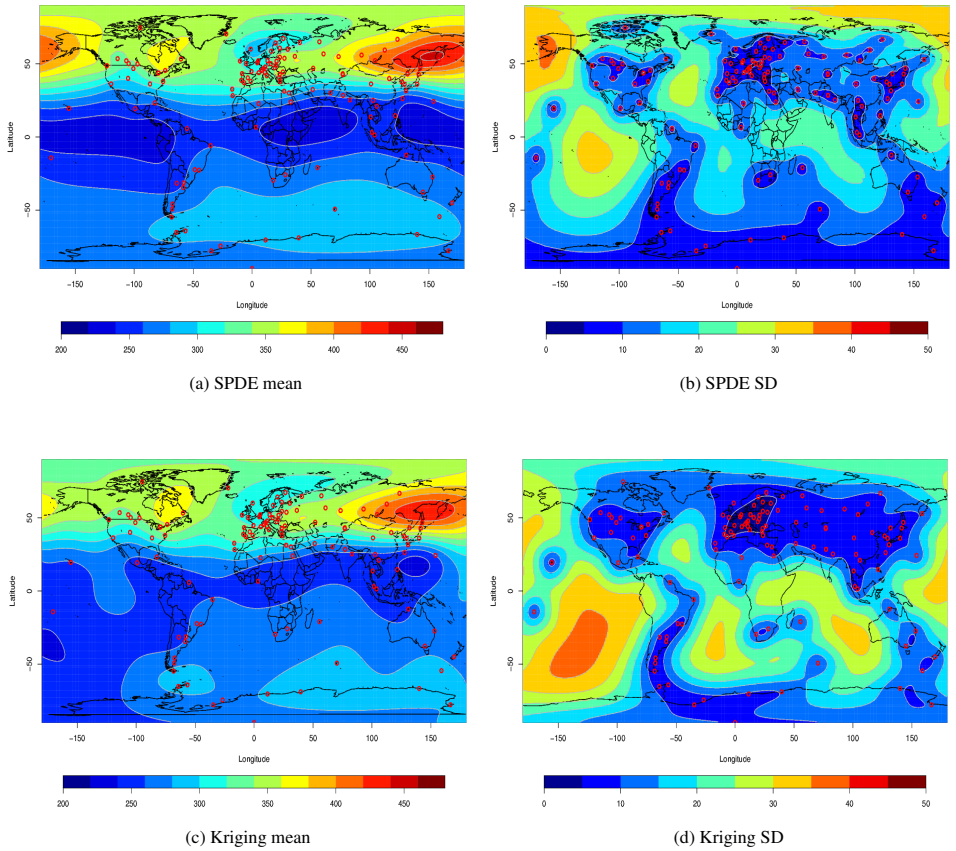

(a) SPDE mean

(b) SPDE SD

(c) Kriging mean

(d) Kriging SD

Figure 1. Surface predicted ozone (DU) mean and SD (SD) for SPDE and kriging on January 2000. The red points indicate the locations of stations.

AMTD
8, 3967–4009, 2015

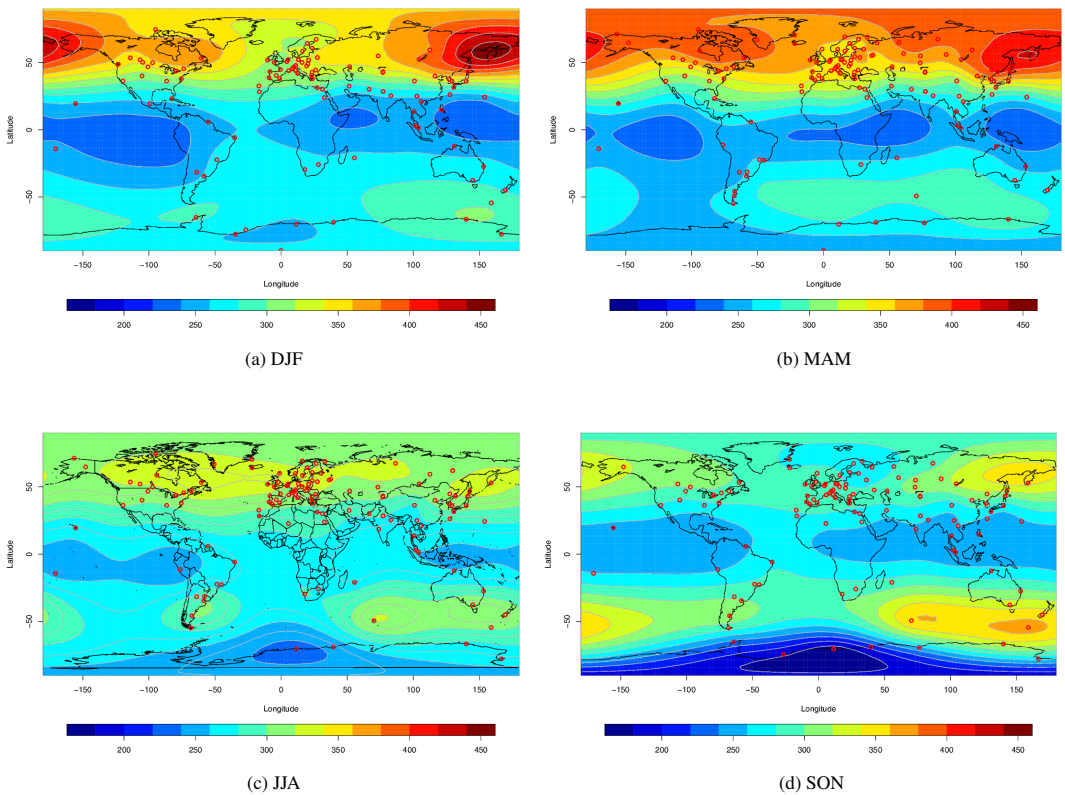

(a) DJF (b) MAM

(c) JJA (d) SON

Figure 2. Surface predicted ozone (DU) mean from SPDE approach by season on 2000.

AMTD
8, 3967–4009, 2015

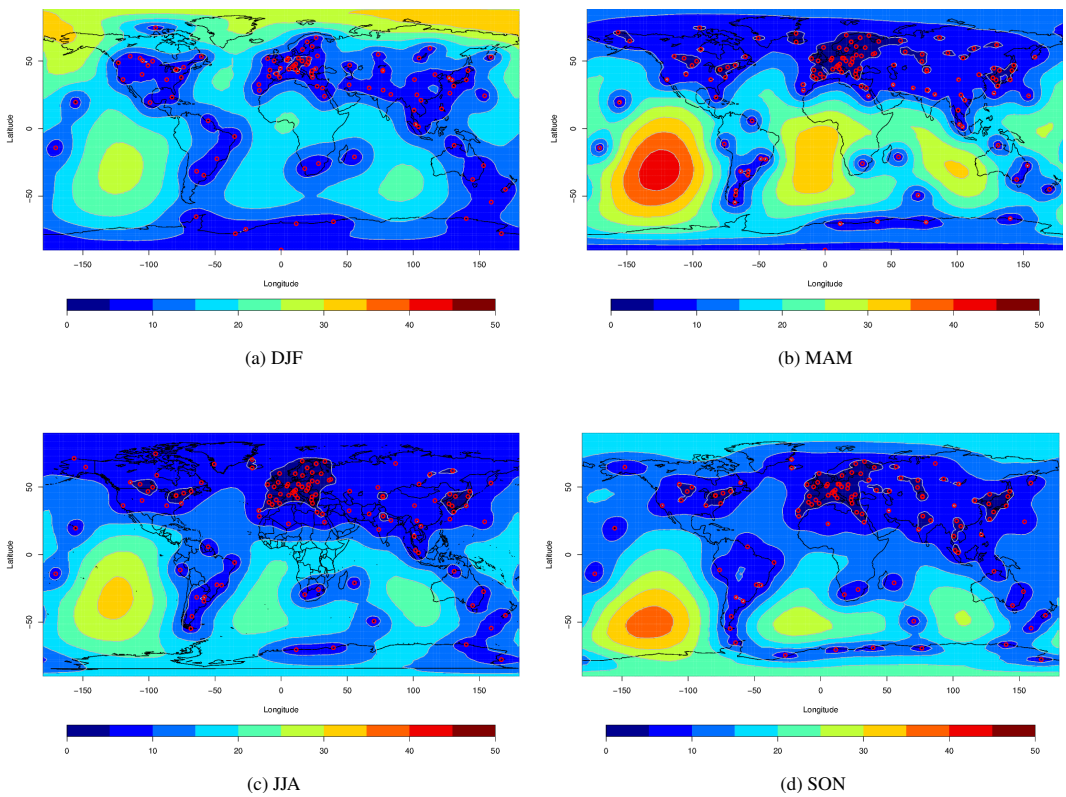

(a) DJF (b) MAM

(c) JJA (d) SON

Figure 3. Surface predicted ozone (DU) SD (SD) from SPDE approach by season on 2000.

AMTD
8, 3967–4009, 2015

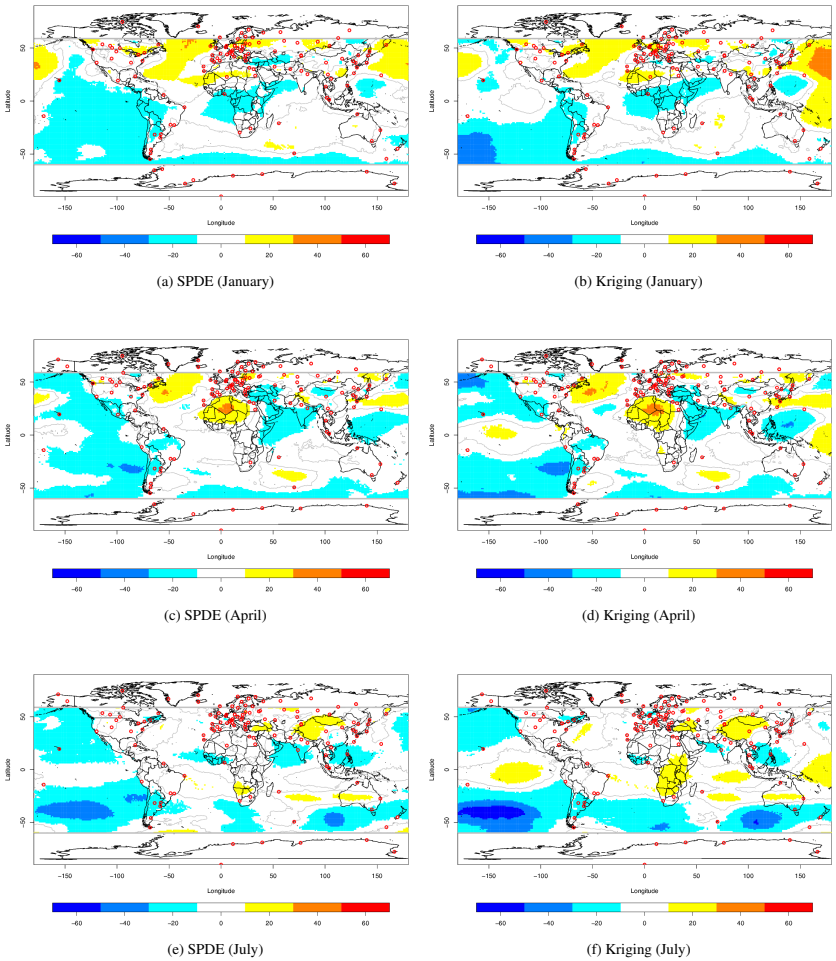

(a) SPDE (January) (b) Kriging (January)

(c) SPDE (April) (d) Kriging (April)

(e) SPDE (July) (f) Kriging (July)

Figure 4. Total ozone (DU) difference mapping of kriging and SPDE estimated mean with respect to satellite data on January, April and July 2000, respectively.

AMTD
8, 3967–4009, 2015

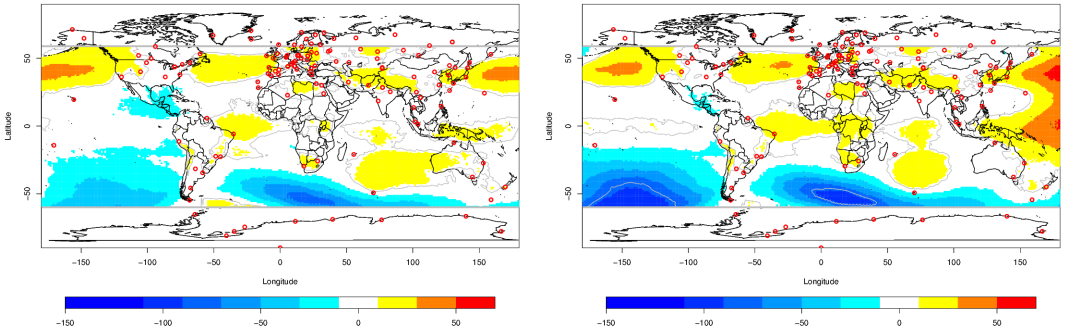

(a) SPDE (October)

(b) Kriging (October)

Figure 5. Total ozone (DU) difference mapping of kriging and SPDE estimated mean with respect to satellite data on October of 2000. Estimation in October shows worse prediction than other months, hence it used different scale from Fig. 4.

AMTD
8, 3967–4009, 2015

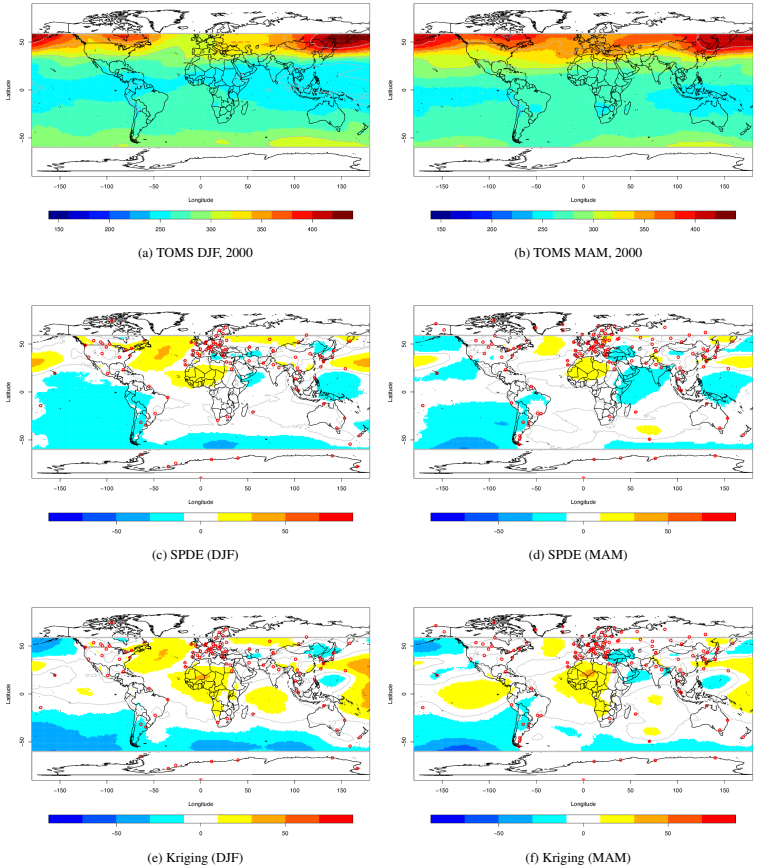

Figure 6. Ozone mapping from TOMS data in **(a)** DJF and **(b)** MAM; global difference mapping of SPDE and kriging predicted mean with respect to TOMS data in DJF (**c** and **e**) and MAM (**d** and **f**), 2000.

AMTD
8, 3967–4009, 2015

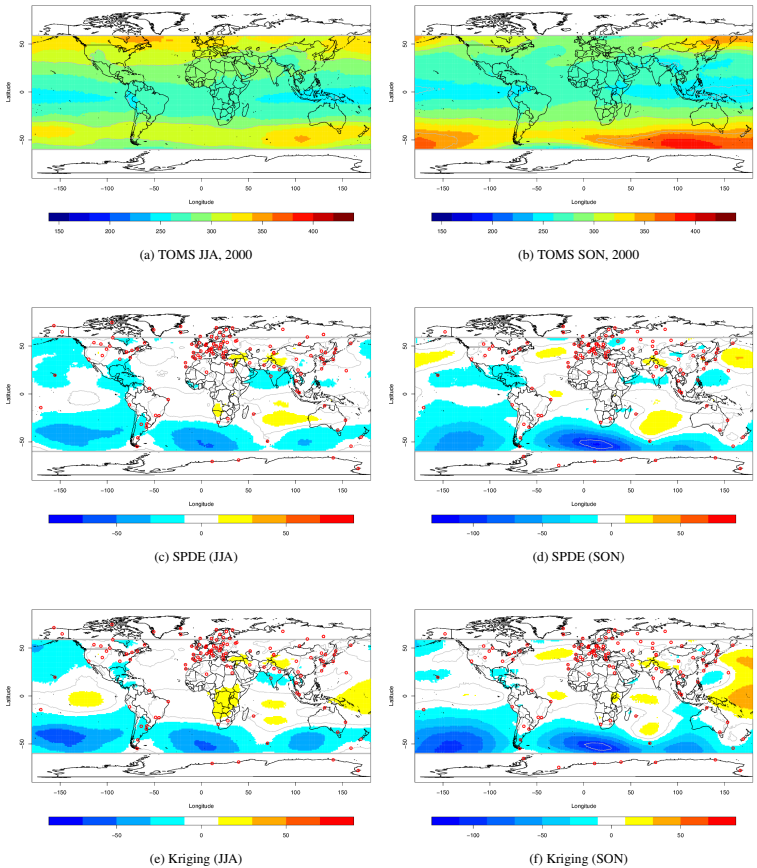

Figure 7. Ozone mapping from TOMS data in **(a)** JJA and **(b)** SON; global difference mapping of SPDE and kriging predicted mean with respect to TOMS data in JJA (**c** and **e**) and SON (**d** and **f**), 2000.

AMTD
8, 3967–4009, 2015

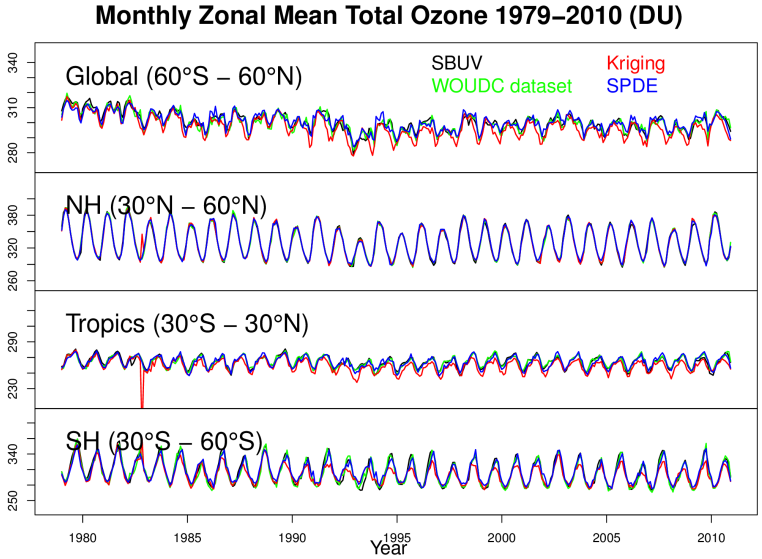

Figure 8. Time series of zonal means by SBUV satellite data (black) WOUDC dataset (green), kriging (red) and SPDE (blue) from 1979–2010.

AMTD
8, 3967–4009, 2015

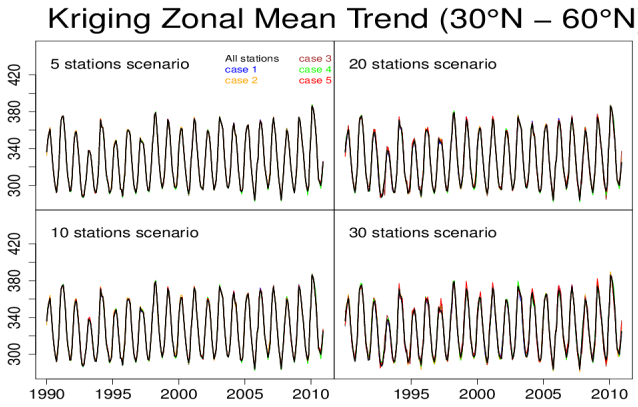

(a) Kriging zonal means (DU)

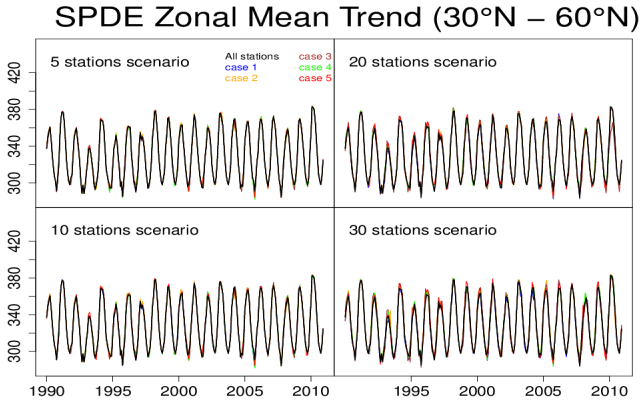

(b) SPDE zonal means (DU)

Figure 9. Time series of 30–60° N zonal means by **(a)** kriging and **(b)** SPDE from 1990–2010 for 4 scenarios with 5, 10, 20, and 30 stations removed globally including 3, 6, 12 and 18 stations removed in the NH respectively.

AMTD
8, 3967–4009, 2015

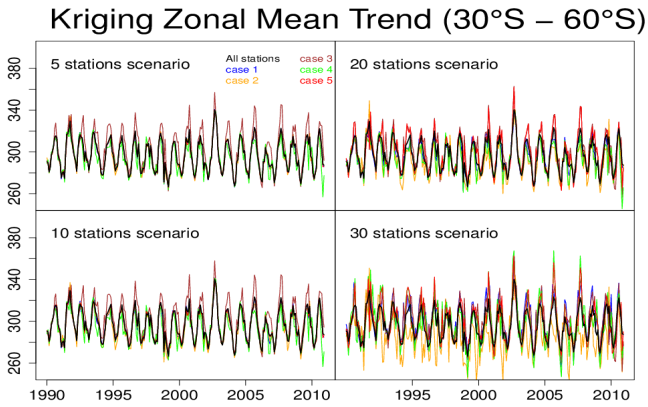

(a) Kriging zonal means (DU)

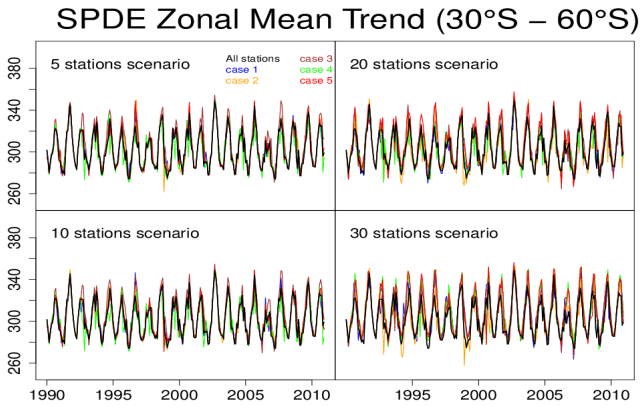

(b) SPDE zonal means (DU)

Figure 10. Time series of 30–60° S zonal means by **(a)** kriging and **(b)** SPDE from 1990–2010 for 4 scenarios with 5, 10, 20, and 30 stations removed globally including 1, 2, 4 and 6 stations removed in the SH respectively.

AMTD
8, 3967–4009, 2015

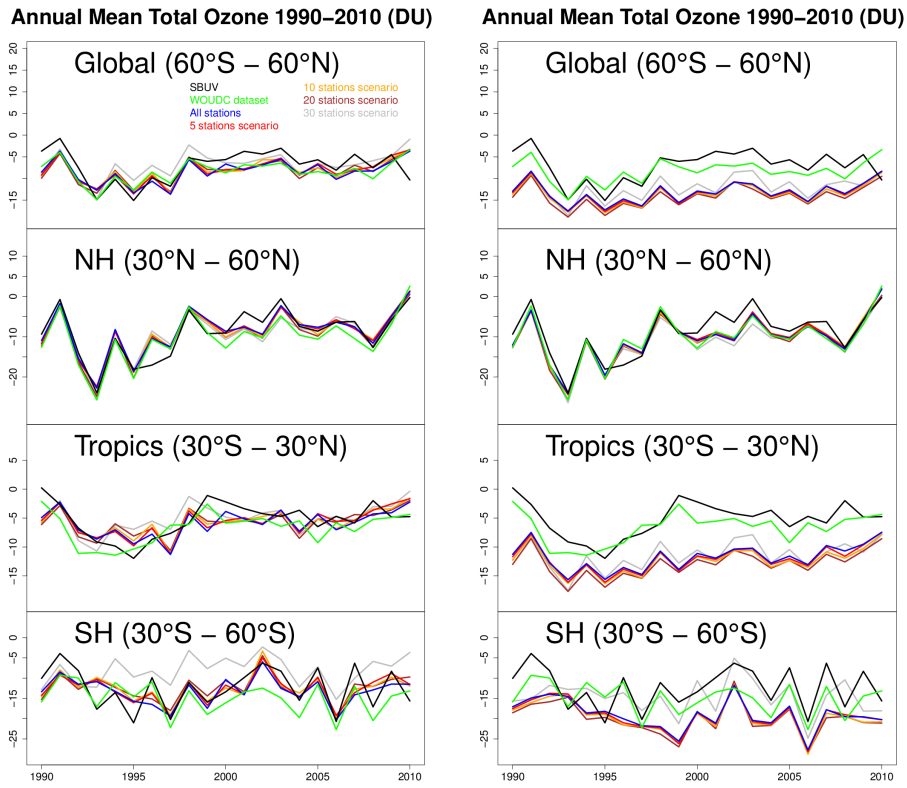

(a) SPDE annual zonal mean

(b) Kriging annual zonal mean

Figure 11. Annual zonal mean deviances from SBUV data (black), WOUDC dataset (green), using all 57 available ground-based data (blue), random removed 5 (red), 10 (yellow), 20 (brown) and 30 (grey) stations in kriging and SPDE estimation over the (1) global (60° N–60° S), (2) NH (30–60° N), (3) Tropics (30° N–30° S), and (4) SH (30–60° S) from 1990–2010.

AMTD
8, 3967–4009, 2015

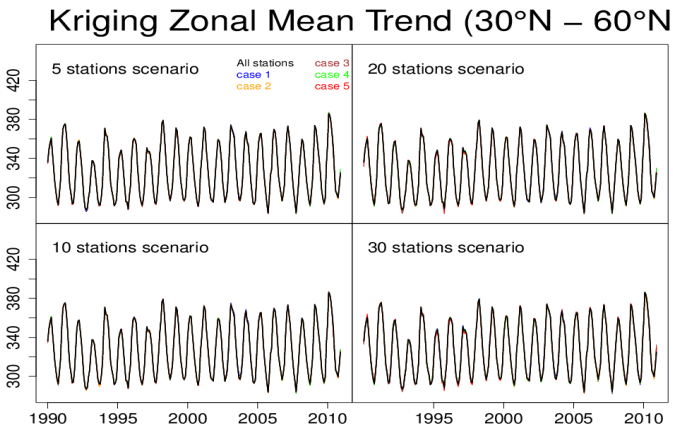

(a) Kriging zonal means (DU)

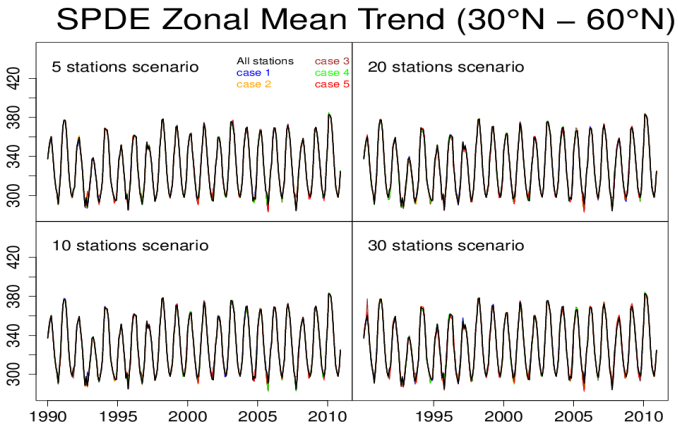

(b) SPDE zonal means (DU)

Figure 12. Time series of 30–60° N zonal means by **(a)** kriging and **(b)** SPDE from 1990–2010 for 4 scenarios with 5, 10, 20, and 30 stations drifted globally.

AMTD
8, 3967–4009, 2015

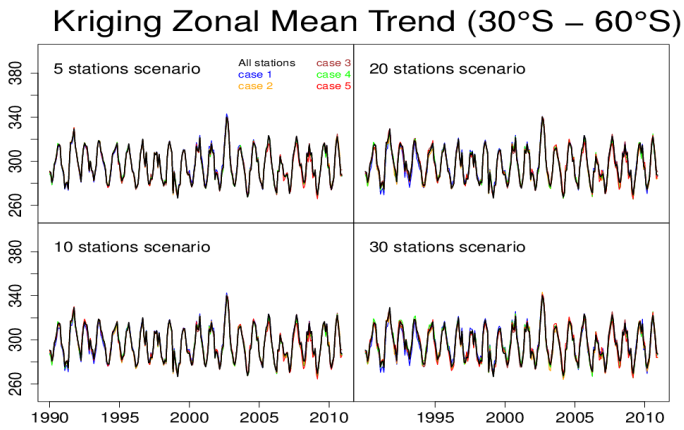

(a) Kriging zonal means (DU)

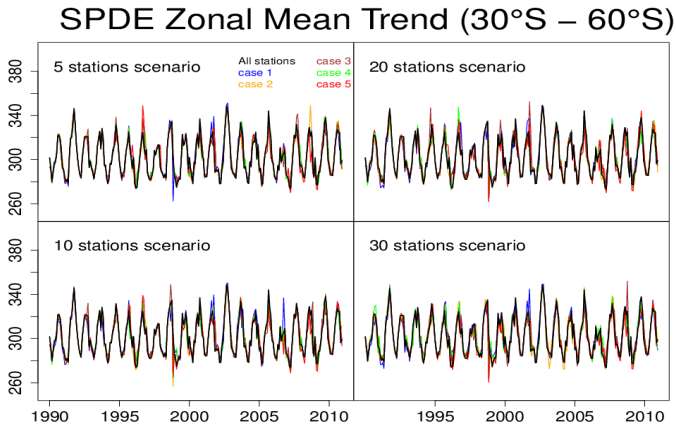

(b) SPDE zonal means (DU)

Figure 13. Time series of 30–60° S zonal means by **(a)** kriging and **(b)** SPDE from 1990–2010 for 4 scenarios with 5, 10, 20, and 30 stations drifted globally.

AMTD
8, 3967–4009, 2015

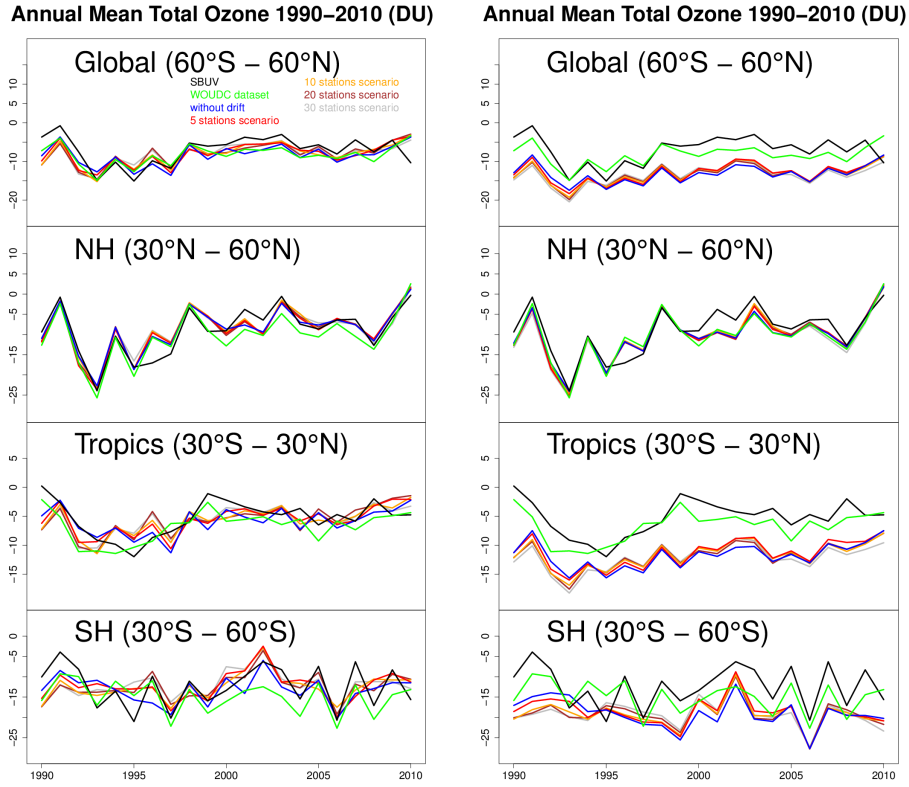

(a) SPDE annual zonal means

(b) Kriging annual zonal means

Figure 14. Annual zonal mean deviances from SBUV data (black), WOUDC dataset (green), using all 57 available ground-based data (blue), adding drift to 5 (red), 10 (yellow), 20 (brown), and 30 (grey) stations in kriging and SPDE estimation over the (1) global (60° N–60° S), (2) NH (30–60° N), (3) Tropics (30° N–30° S), and (4) SH (30–60° S) from 1990–2010.

AMTD
8, 3967–4009, 2015